

In Vitro and *In Vivo* Comparison of 3,2-HOPO Versus Deferoxamine-Based Chelation of Zirconium-89 to the Antimesothelin Antibody Anetumab

Jyoti Roy,¹ Elaine M. Jagoda,¹ Falguni Basuli,² Olga Vasalatiy,² Tim E. Phelps,¹ Karen Wong,¹ Anita T. Ton,¹ Urs B. Hagemann,³ Alan S. Cuthbertson,⁴ Patricia E. Cole,⁵ Raffit Hassan,⁶ Peter L. Choyke,¹ and Frank I. Lin¹

Abstract

Introduction: [²²⁷Th]Th-3,2-HOPO-MSLN-mAb, a mesothelin (MSLN)-targeted thorium-227 therapeutic conjugate, is currently in phase I clinical trial; however, direct PET imaging using this conjugate is technically challenging. Thus, using the same MSLN antibody, we synthesized 3,2-HOPO and deferoxamine (DFO)-based zirconium-89 antibody conjugates, [⁸⁹Zr]Zr-3,2-HOPO-MSLN-mAb and [⁸⁹Zr]Zr-DFO-MSLN-mAb, respectively, and compared them *in vitro* and *in vivo*.

Methods: [⁸⁹Zr]Zr-3,2-HOPO-MSLN-mAb and [⁸⁹Zr]Zr-DFO-MSLN-mAb were evaluated *in vitro* to determine binding affinity and immunoreactivity in HT29-MSLN and PDX (NCI-Meso16, NCI-Meso21) cells. For both the zirconium-89 conjugates, *in vivo* studies (biodistribution/imaging) were performed at days 1, 3, and 6, from which tissue uptake was determined.

Results: Both the conjugates demonstrated a low nanomolar binding affinity for MSLN and >95% immunoreactivity. In all the three tumor types, biodistribution of [⁸⁹Zr]Zr-DFO-MSLN-mAb resulted in higher tumor uptake (15.88-28-33%ID/g) at all time points compared with [⁸⁹Zr]Zr-3,2-HOPO-MSLN-mAb (7-13.07%ID/g). [⁸⁹Zr]Zr-3,2-HOPO-MSLN-mAb femur uptake was always higher than [⁸⁹Zr]Zr-DFO-MSLN-mAb, and imaging results concurred with the biodistribution studies.

Conclusions: Even though the conjugates exhibited a high binding affinity for MSLN, [⁸⁹Zr]Zr-DFO-MSLN-mAb showed a higher tumor and lower femur uptake than [⁸⁹Zr]Zr-3,2-HOPO-MSLN-mAb. Nevertheless, [⁸⁹Zr]Zr-3,2-HOPO-MSLN-mAb could be used to study organ distribution and lesion uptake with the caveat of detecting MSLN-positive bone lesions. Clinical trial (NCT03507452).

Keywords: 32-HOPO, antibody conjugate, DFO, mesothelin, PET imaging, zirconium-89

Introduction

Targeted alpha therapy (TAT) is a promising new cancer therapy, which induces DNA double-stranded breaks in cancer cells, by specific delivery of alpha particle emitting radionuclide-labeled tracers to tumors.¹⁻⁶ At present, several α -particle emitting radionuclides with suitable half-lives are under evaluation for TATs.^{5,7-9} Thorium-227 has been

evaluated to develop TAT for treating various cancers.⁹⁻¹⁵ Targeted thorium-227 conjugates (TTCs) have demonstrated promising preclinical therapeutic results in acute myeloid leukemia, ovarian, breast, pancreatic, lung, and renal cell carcinoma xenografts.^{10-13,15}

Mesothelin (MSLN) antibody-targeted thorium-227 conjugate (MSLN-TTC; ²²⁷Th-anetumab corixetan) has been developed for treating MSLN-positive cancers. MSLN is a

¹Molecular Imaging Program, National Cancer Institute, National Institutes of Health, Bethesda, Maryland, USA.

²Chemistry and Synthesis Center, National Heart, Lung, and Blood Institute, National Institutes of Health, Rockville, Maryland, USA.

³Bayer AG, Pharmaceutical Division, Berlin, Germany.

⁴Bayer AS, Thorium Conjugate Research, Oslo, Norway.

⁵Bayer USA, LLC, Whippany, New Jersey, USA.

⁶Thoracic and GI Malignancies Branch, National Cancer Institute, National Institutes of Health, Bethesda, Maryland, USA.

Address correspondence to: Frank I. Lin; Molecular Imaging Program, National Cancer Institute, National Institutes of Health; Building 10, Room # B3B69F, Bethesda, MD 20892, USA
E-mail: frank.lin2@nih.gov

© Jyoti Roy et al. 2021; Published by Mary Ann Liebert, Inc. This Open Access article is distributed under the terms of the Creative Commons Attribution Noncommercial License [CC-BY-NC] (<http://creativecommons.org/licenses/by-nc/4.0/>) which permits any non-commercial use, distribution, and reproduction in any medium, provided the original author(s) and the source are cited.

GPI-anchored glycoprotein known to be overexpressed in malignant mesothelioma, lung, ovarian, pancreatic, breast, gastric, head and neck cancers with restricted expression in healthy tissues.^{16–19} MSLN-TTC was developed by covalently conjugating a fully humanized MSLN-mAb (anetumab, BAY861903) to 3-hydroxypyridin-2-one (3,2-HOPO) chelator and radiolabeling it with thorium-227 to produce [²²⁷Th]Th-3,2-HOPO-MSLN-mAb (BAY 2287411).^{11,20}

In vivo [²²⁷Th]Th-3,2-HOPO-MSLN-mAb has demonstrated therapeutic efficacy in various cancers.^{9–14} In a study, BAY2287411 in combination with ATR (BAY1895344) and PARP (Olaparib/AZD2281) inhibitors demonstrated synergistic antitumor effects in ovarian cancer xenografts.¹⁰ Currently, [²²⁷Th]Th-3,2-HOPO-MSLN-mAb is under evaluation for safety and tolerability in a multicenter phase I clinical trial (NCT03507452).

Due to the low γ -emission and low abundance of measurable photons in the decay chain of thorium-227, direct imaging using [²²⁷Th]Th-3,2-HOPO-MSLN-mAb is technically challenging. However, 3,2-HOPO chelator has been shown to form thermodynamically stable complexes with thorium-227 and zirconium-89.^{14,21–23} Thus, the same 3,2-HOPO-MSLN-mAb can be radiolabeled with thorium-227 for therapeutic or zirconium-89 for PET imaging agents. Zirconium-89 based conjugate may enable identification of MSLN-positive tumor lesions as well as study biodistribution of the MSLN antibody conjugate.

Even though there are several other chelators that can be used with zirconium-89, deferoxamine (DFO) is one of the most widely used chelators of zirconium-89 that is currently used for PET imaging in both preclinical and clinical settings.^{24–32} Therefore, in the present work, we synthesized [⁸⁹Zr]Zr-HOPO-MSLN-mAb and [⁸⁹Zr]Zr-DFO-MSLN-mAb, and evaluated both the conjugates *in vitro* and *in vivo* in three different tumor xenografts. *In vitro* serum stability of these conjugates was also determined. The results of this study may help evaluate [⁸⁹Zr]Zr-3,2-HOPO-MSLN-mAb and [⁸⁹Zr]Zr-DFO-MSLN-mAb as PET imaging agents.

Methods

All studies were done on protocols approved by the NIH Animal Care and Use Committee.

Synthesis of ([⁸⁹Zr]Zr-3,2-HOPO-MSLN-mAb)

A mixture of zirconium-89 (IV) (~ 37 MBq, ~ 1 mCi) and 3,2-HOPO-MSLN-mAb (65 μ g) was incubated for 1 h at room temperature and purified by PD-10 column to obtain [⁸⁹Zr]Zr-3,2-HOPO-MSLN-mAb. A detailed description of the radiolabeling procedure and *in vitro* serum stabilities is provided in the Supplementary Data.

Synthesis of ([⁸⁹Zr]Zr-DFO-MSLN-mAb)

The DFO-MSLN-mAb conjugate was prepared following a published literature method using a threefold molar excess of chelator (DFO-Bz-NCS)³³ with respect to MSLN-mAb. The chelators per antibody ratio (CAR, 0.8) was determined by radiometric isotope dilution assay.³⁴ [⁸⁹Zr]Zr-DFO-MSLN-mAb was prepared according to the literature method using ~ 74 MBq (~ 2 mCi) zirconium-89 (IV) and 300 μ g DFO-MSLN-mAb.^{26,33}

In vitro saturation and competition assays

For saturation studies, NCI-Meso16, NCI-Meso21, and HT29-MSLN cells were aliquoted at a constant concentration (250,000–500,000 cells/tube) into tubes containing six concentrations of radiolabeled antibody [⁸⁹Zr]Zr-DFO-MSLN-mAb (0.4–16 nM) or [⁸⁹Zr]Zr-3,2-HOPO-MSLN-mAb (1–35 nM); nonspecific binding was determined in the presence of 1 μ M concentration of unlabeled MSLN-mAb by adding the cells to the same concentrations ([⁸⁹Zr]Zr-DFO-MSLN-mAb:0.4–16 nM; [⁸⁹Zr]Zr-3,2-HOPO-MSLN-mAb:1–35 nM) of radiolabeled MSLN-mAb conjugates.

For the competition assay, the same number of cells was added to each tube and incubated with a constant concentration of [⁸⁹Zr]Zr-DFO-MSLN-mAb or [⁸⁹Zr]Zr-3,2-HOPO-MSLN-mAb in the presence of various concentrations of the unlabeled MSLN-mAb (10^{-6} – 10^{-12} M). After 2 h incubation on ice, the cells from both saturation and competition assays were centrifuged and washed twice with cold PBS to separate bound radiolabeled MSLN-Ab conjugate from unbound. Cell bound radioactivity in the cell pellet was determined by γ -counting (PerkinElmer 2480 Wizard3).

The K_d and B_{max} were determined from nonlinear regression curve fit (one-site binding hyperbola, GraphPad Prism 7) from six different concentrations of [⁸⁹Zr]Zr-DFO-MSLN-mAb or [⁸⁹Zr]Zr-3,2-HOPO-MSLN-mAb. The immunoreactive fraction of the radiolabeled antibodies [⁸⁹Zr]Zr-DFO-MSLN-mAb or [⁸⁹Zr]Zr-3,2-HOPO-MSLN-mAb were determined by the Morris method as previously described.³⁵ In brief, the immunoreactivity was derived from saturation and self-displacement assay data.³³

Mouse tumor models

Athymic female nude mice (NCr-nu/nu, 4- to 6-week old, Charles River) were inoculated in the right shoulder by subcutaneous injection of NCI-Meso16 (8×10^6 cells), NCI-Meso21 (10×10^6 cells), or HT29-MSLN (2×10^6 cells) cancer cells in RPMI:Matrigel (50:50).³⁶ Mice were housed under 12:12 light/day cycles, and given standard rodent chow and water *ad libitum*. All the studies and experiments were performed following approved protocols by NIH ACUC.

Biodistribution studies

Tumor-bearing mice (NCI-Meso16, NCI-Meso21, or HT29-MSLN; 200–400 mm³) were injected 1 d before radiolabeled MSLN-mAb conjugate injections with irrelevant IgG2a antibody (200 μ g; Sigma) to block the unspecific accumulation of the MSLN-mAb in the spleen.³⁷ Mice were intravenously injected with 1.85 MBq (50 μ Ci) of either [⁸⁹Zr]Zr-3,2-HOPO-MSLN-mAb or [⁸⁹Zr]Zr-DFO-MSLN-mAb and euthanized (CO₂ asphyxiation) at days 1, 3, and 6. Blood and tissue samples were collected and weighed, and associated radioactivity (counts per minute, CPM) was determined using a γ -counter (Perkin Elmer 2480 Wizard3). The data were calculated as % injected dose per gram (%ID/g) of the tissue normalized to 20 g mice, tissue:blood ratios, tissue:muscle ratios using the following formula:

$$\%ID/g \text{ normalized to 20g mice} = \frac{CPM_{\text{tissue}} \times \text{body weight(g)} \times 100}{\text{tissue weight(g)} \times CPM_{\text{injected dose}} \times 20(\text{g})}$$

$$\text{Tissue:Blood Ratios} = \frac{(\% \text{ Injected dose per gram})_{\text{tissue}}}{(\% \text{ Injected dose per gram})_{\text{blood}}}$$

$$\text{Tissue:Muscle Ratios} = \frac{(\% \text{ Injected dose per gram})_{\text{tissue}}}{(\% \text{ Injected dose per gram})_{\text{muscle}}}$$

For the blocking study, a separate group of HT29-MSLN tumor-bearing mice were injected with [⁸⁹Zr]Zr-3,2-HOPO-MSLN-mAb (1.85 MBq, 50 μCi, 4.5 μg) in the presence or absence of an excess of the unlabeled 3,2-HOPO-MSLN-mAb (180 μg). Mice were euthanized and biodistribution was performed 3 d postinjections, and radioactivity associated with organs/tissues was counted using a gamma counter (Perkin Elmer 2480 Wizard3).

MicroPET/CT imaging studies

Tumor-bearing mice were injected with 1.85 MBq (50 μCi, i.v.) of either [⁸⁹Zr]Zr-3,2-HOPO-MSLN-mAb or [⁸⁹Zr]Zr-DFO-MSLN-mAb. HT29-MSLN tumor-bearing mice were anesthetized using isoflurane/O₂ (1.5–3%v/v) and imaged at 1, 3, or 6 d. NCI-Meso16 and NCI-Meso21 mouse xenografts were only imaged 3 d postinjection of the radioactive conjugates. Whole-body static images were obtained using the BioPET scanner, following these parameters: 2 bed positions, FOV=2.0 cm, image time=10. CT scans of the mice were obtained by using the parameters: X-ray=180, voltage (kV)=50, # projection=360. The PET/CT images were reconstructed and coregistered to present the data.

Data analysis

Data analysis for the *in vitro* assay was performed using GraphPad Prism7 and TableCurve2D v5.01. *In vivo* PET/CT images were reconstructed using MIM software. A significance test was performed using the Student *t*-test.

Results

Conjugation, radiochemistry, and serum stability

The initial radiolabeling of the 3,2-HOPO-MSLN-mAb conjugate (Fig. 1A) was conducted according to the literature method reported for the zirconium-89 labeling of DFO using ~1 mCi of zirconium-89 and 130 μg of 3,2-HOPO-MSLN-mAb in a total volume of 0.25 mL.³³ A high radiochemical yield (80%–85%) was observed; however, the amount of aggregate (30%) was also high. To minimize the amount of aggregate variable ratio of zirconium-89 to 3,2-HOPO-MSLN-mAb was tested. The results indicated that optimum radiochemical yield was obtained when ~1 mCi of zirconium-89 was incubated with 65 μg of 3,2-HOPO-MSLN-mAb in a total volume of 1 mL.

DFO-MSLN-mAb conjugate (Fig. 1B) was radiolabeled with zirconium-89 to prepare [⁸⁹Zr]Zr-DFO-MSLN-mAb.³³ The isolated radiochemical yields were in the range of 52%–76% (*n*=20) for [⁸⁹Zr]Zr-3,2-HOPO-MSLN-mAb and

90%–92% (*n*=8) for [⁸⁹Zr]Zr-DFO-MSLN-mAb. The molar activities of the conjugates were 22,200–77,700 MBq/μmol (600–2100 mCi/μmol) with 82%–95% radiochemical purity (Fig. 1C, D). HPLC chromatogram (size exclusion) at 280 nm indicated the presence of 5%–18% aggregation.

In vitro serum stability of the conjugates was tested in a whole human serum over 4 d (Supplementary Table S1) at 37°C. The SE-HPLC chromatogram revealed the gradual decomposition of both the radiolabeled conjugates. No significant differences in the amount of intact conjugates were observed between the two conjugates on days 1 and 2 (Supplementary Figure S1 and S2). However, by day 4, the amount of intact [⁸⁹Zr]Zr-DFO-MSLN-mAb (46%) was twice the amount of intact [⁸⁹Zr]Zr-3,2-HOPO-MSLN-mAb (23%). The *in vitro* serum stability study indicated slower decomposition of [⁸⁹Zr]Zr-DFO-MSLN-mAb after 2 d of incubation at 37°C. HPLC chromatogram indicated that the major decomposition product (~12 min) of [⁸⁹Zr]Zr-3,2-HOPO-MSLN-mAb is different from the major decomposition product (~15 min) of [⁸⁹Zr]Zr-DFO-MSLN-mAb. However, no attempts were made to characterize those decomposition products.

In vitro binding studies

Compared with NCI-Meso21 (341×10³ MSLN per cell) and HT29-MSLN cells (249×10³ MSLN per cell), NCI-Meso16 cells (178.41×10³ MSLN per cell) expressed relatively low levels of MSLN (Fig. 3A). In NCI-Meso16, NCI-Meso21, and HT29-MSLN cells, [⁸⁹Zr]Zr-DFO-MSLN-mAb exhibited K_d of 0.16±0.02 nM, 0.29±0.02 nM, and 0.59±0.06 nM, respectively, for MSLN (Figs. 2 and 3B). In the same cancer cell lines, the binding affinity of [⁸⁹Zr]Zr-3,2-HOPO-MSLN-mAb conjugate for MSLN was found to be 2.1±0.09 nM (NCI-Meso16), 2.3±0.46 nM (NCI-Meso21), and 1.9±0.39 nM (HT29-MSLN; Figs. 2 and 3B).

Even though both the conjugates exhibited high binding affinity, the affinity of [⁸⁹Zr]Zr-DFO-MSLN-mAb for MSLN was significantly higher (*p*<0.05) than [⁸⁹Zr]Zr-3,2-HOPO-MSLN-mAb. In all the three cell lines, uptake of both the radiolabeled MSLN-mAb conjugates could be blocked in the presence of unlabeled MSLN-mAb, indicating MSLN-mediated uptake of the conjugates (Fig. 2). The immunoreactivity for [⁸⁹Zr]Zr-DFO-MSLN-mAb and [⁸⁹Zr]Zr-3,2-HOPO-MSLN-mAb was determined to be 95% and 96%, respectively (Fig. 4).

In vivo biodistribution and imaging studies

Pharmacokinetics of [⁸⁹Zr]Zr-3,2-HOPO-MSLN-mAb were determined in HT29-MSLN xenografts for 6 d (Fig. 5A). The uptake of [⁸⁹Zr]Zr-3,2-HOPO-MSLN-mAb in nontarget tissues either declined or remained the same over the study period except for the femur. Among the nontarget tissues, the highest uptake was observed in the femur, which significantly increased (day 1: 6.74%ID/g; day 3: 16.52%ID/g; day 6: 15.40%ID/g) over the 6 d (Fig. 5A). Radioactive accumulation in the femur may likely indicate loss of free zirconium-89 from the conjugate, which can be scavenged by the bone.^{38,39}

[⁸⁹Zr]Zr-3,2-HOPO-MSLN-mAb was retained in the HT29-MSLN tumors from day 1 (10.67%ID/g) through day 3 (11.67%ID/g). Compared with days 1 and 3, tumor uptake of [⁸⁹Zr]Zr-3,2-HOPO-MSLN-mAb declined to 7.97%ID/g

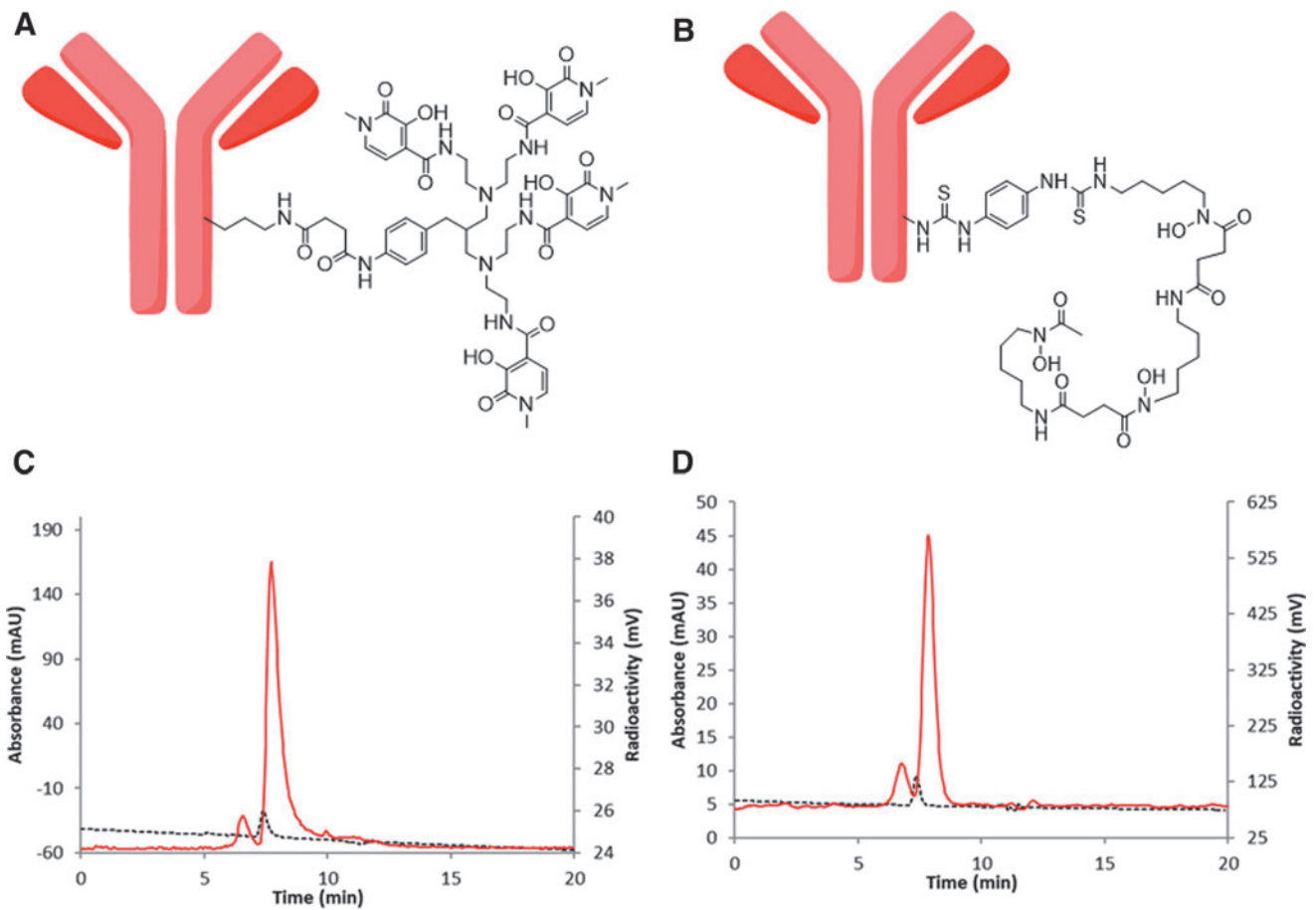


FIG. 1. Structure of antibody conjugate and HPLC result. Structure of mesothelin antibody–chelator conjugate, 3,2-HOPO-MSLN-mAb (A) and DFO-MSLN-mAb. (B) Representative HPLC of zirconium-89 labeled conjugates, $[^{89}\text{Zr}]\text{Zr}$ -3,2-HOPO-MSLN-mAb (C), and $[^{89}\text{Zr}]\text{Zr}$ -DFO-MSLN-mAb. (D) HPLC condition: eluent, 0.1 M sodium phosphate, 0.1 M sodium sulfate, 0.05% sodium azide, 10% isopropyl alcohol (pH 6.8), flow rate 0.3 mL/min; black line UV detector, red line radiodetector.

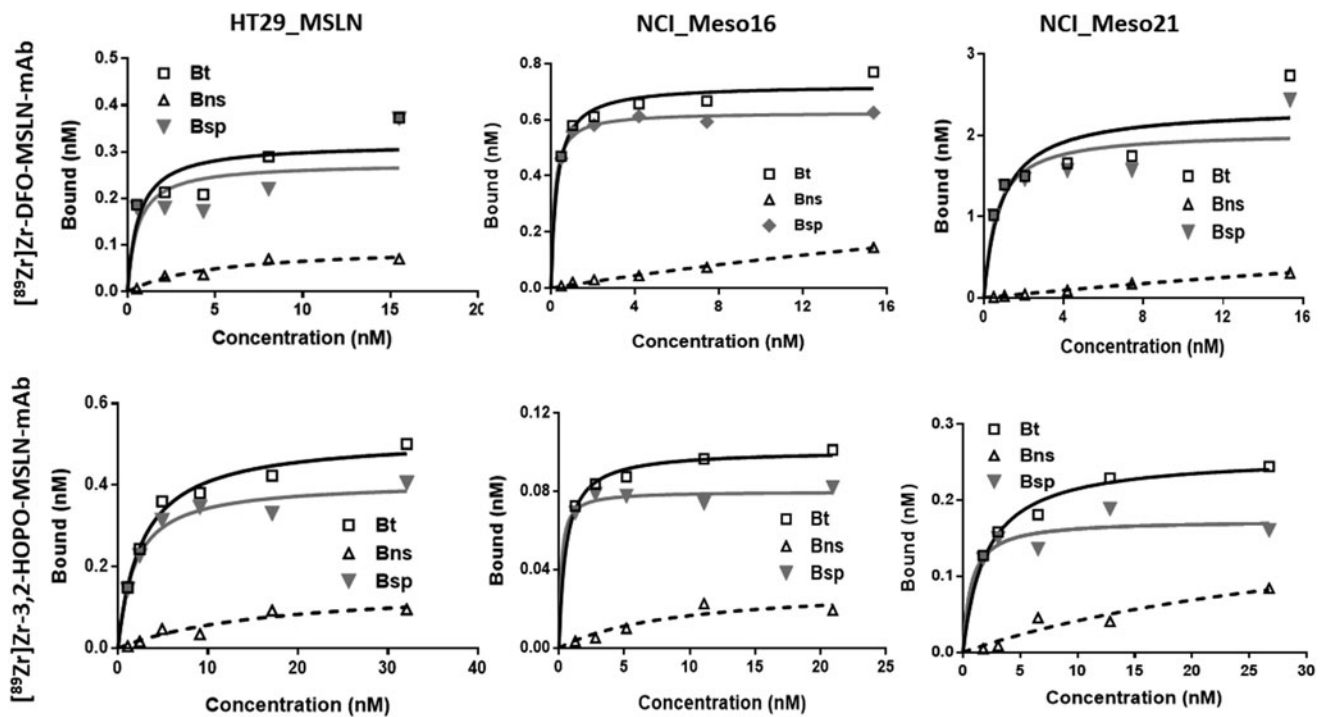


FIG. 2. *In vitro* saturation assay graphs. Representative *in vitro* saturation graphs of $[^{89}\text{Zr}]\text{Zr}$ -3,2-HOPO-MSLN-mAb and $[^{89}\text{Zr}]\text{Zr}$ -DFO-MSLN-mAb in HT29-MSLN, NCI-Meso16, and NCI-Meso21. For each plot Bt, bound total; Bns, bound nonspecific; Bsp, bound specific (Bt=Bns+Bsp).

A		B		
Cell Line	Mesothelin/Cell (10^3)	Cell Line	Radiolabeled Antibody	K_d (nM)
NCI-Meso16	178	NCI-Meso16	$[^{89}\text{Zr}]\text{Zr-DFO-MSLN-mAb}$	0.16 ± 0.02
NCI-Meso21	341	NCI-Meso21	$[^{89}\text{Zr}]\text{Zr-DFO-MSLN-mAb}$	0.29 ± 0.02
HT29-MSLN	249	HT29-MSLN	$[^{89}\text{Zr}]\text{Zr-DFO-MSLN-mAb}$	0.59 ± 0.06
		NCI-Meso16	$[^{89}\text{Zr}]\text{Zr-3,2-HOPO-MSLN-mAb}$	2.1 ± 0.09
		NCI-Meso21	$[^{89}\text{Zr}]\text{Zr-3,2-HOPO-MSLN-mAb}$	2.3 ± 0.46
		HT29-MSLN	$[^{89}\text{Zr}]\text{Zr-3,2-HOPO-MSLN-mAb}$	1.9 ± 0.39

FIG. 3. Mesothelin density per cell and binding affinity. Number of mesothelin per cell (A) and binding affinities (B; K_d) of $[^{89}\text{Zr}]\text{Zr-3,2-HOPO-MSLN-mAb}$ and $[^{89}\text{Zr}]\text{Zr-DFO-MSLN-mAb}$ for mesothelin were derived from the *in vitro* saturation assays in HT29-MSLN, NCI-Meso16, and NCI-Meso21 cells. The assay was performed on an average two to three times for each cell type.

on day 6 (Fig. 5A). Since radioactivity in the blood (%ID/g) decreased over the study period, Tissue:Blood ratios were calculated to normalize the difference in the input function. Tissue:Blood ratios (T:B; Fig. 5B) for tumor (day 1: 0.63; day 3: 1.22; day 6: 2.83) and femur (day 1: 0.37; day 3: 1.97; day 6: 5.06) increased over the study period with the highest ratios observed on day 6.

Since MSLN is not expressed in muscle, radioactivity associated with muscle was considered as background, thus Tissue:Muscle ratio was calculated to account for any interference

due to background tissue radioactivity. Tissue:Muscle (T:M) ratios for tumor and femur increased over 6 d (Fig. 5C); however, this increasing T:M ratio is likely more indicative of the increased clearance of the radioactive conjugate from the muscle rather than an increased uptake in the tissue since the %ID/g in muscle decreased over the 6 d period. Approximately 80% (Fig. 5E) of the tumor uptake of $[^{89}\text{Zr}]\text{Zr-3,2-HOPO-MSLN-mAb}$ could be blocked by the administration of excess of 3,2-HOPO-MSLN-mAb, indicating MSLN mediated accumulation of $[^{89}\text{Zr}]\text{Zr-3,2-HOPO-MSLN-mAb}$ in the tumor.

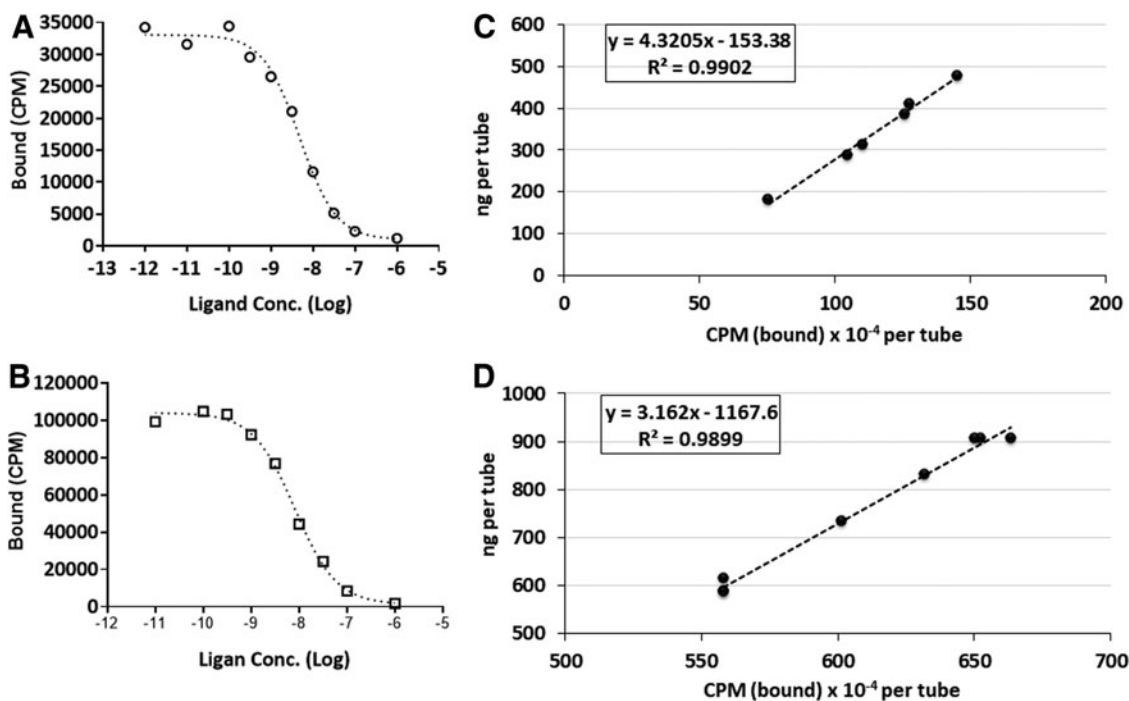


FIG. 4. Competition binding assay and immunoreactivity plots. Representative plots from an *in vitro* $[^{89}\text{Zr}]\text{Zr-3,2-HOPO-MSLN-mAb}$ (A) and $[^{89}\text{Zr}]\text{Zr-DFO-MSLN-mAb}$, (B) competition-binding assays using unlabeled MSLN targeted monoclonal antibody (self-displacement, Morris method) with HT29-MSLN cells. Each point (average of duplicates) represents cell-bound CPM. Representative plots for determination of the % immunoreactivity (immunoreactive fraction) of $[^{89}\text{Zr}]\text{Zr-3,2-HOPO-MSLN-mAb}$ (C) and $[^{89}\text{Zr}]\text{Zr-DFO-MSLN-mAb}$ (D) from the same batch by the Morris method: representative plot (linear regression curve fit), immunoreactivity for $[^{89}\text{Zr}]\text{Zr-3,2-HOPO-MSLN-mAb}$ =96% and $[^{89}\text{Zr}]\text{Zr-DFO-MSLN-mAb}$ =95%. CPM, count per minute.

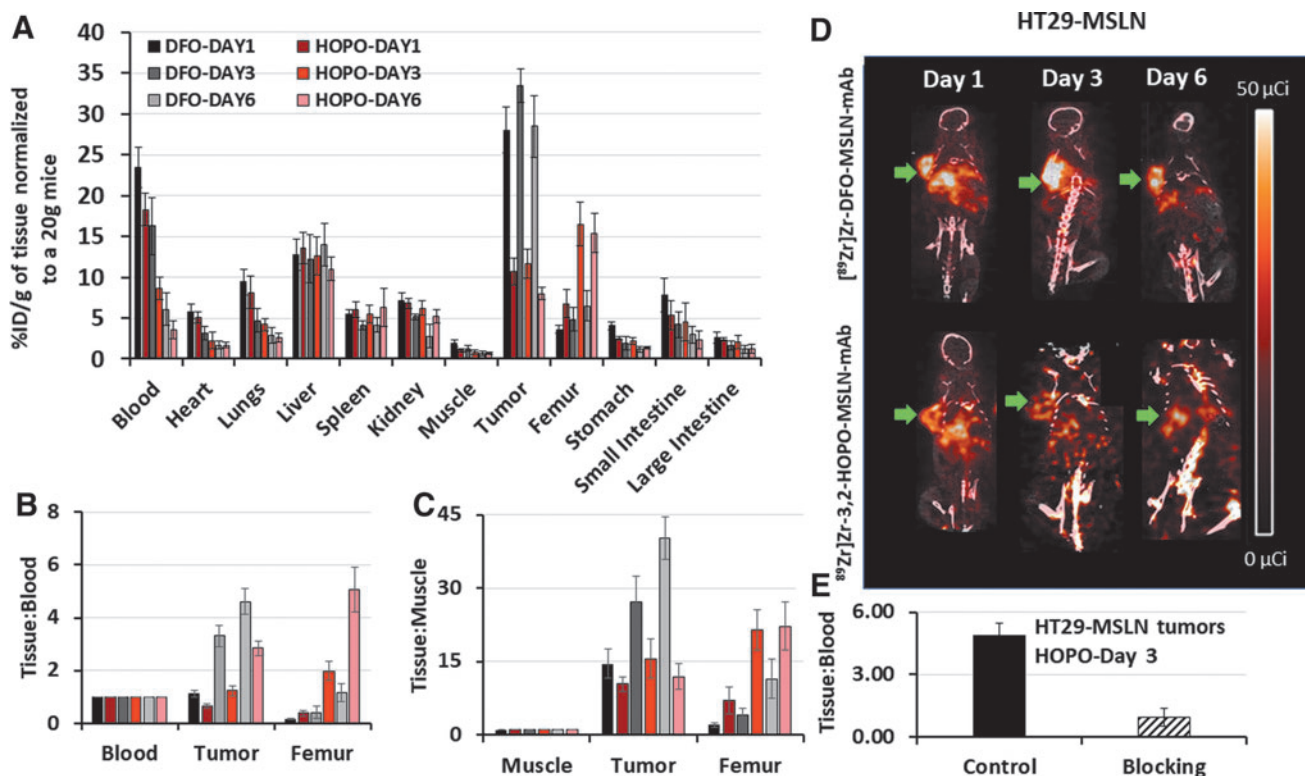


FIG. 5. Biodistribution and PET imaging. Biodistribution (A) of [^{89}Zr]Zr-3,2-HOPO-MSLN-mAb (HOPO) and [^{89}Zr]Zr-DFO-MSLN-mAb (DFO) in HT29-MSLN xenografts from 1 to 6 d. Each point represents the mean %ID/g of tissue normalized to 20 g mice \pm SE ($n=9$, 10 for each point). Tissue:Blood ratios (B) and Tissue:Muscle ratios (C) of [^{89}Zr]Zr-3,2-HOPO-MSLN-mAb (HOPO) and [^{89}Zr]Zr-DFO-MSLN-mAb (DFO) in tumor and femur over a period of 6 d. Each point represents the mean ratio \pm SE ($n=9$, 10 for each point). Representative coronal PET/CT images (D) of HT29-MSLN mouse xenografts at days 1, 3, and 6 postinjection of (50 μCi , 1.85 MBq) of [^{89}Zr]Zr-3,2-HOPO-MSLN-mAb and [^{89}Zr]Zr-DFO-MSLN-mAb. Green arrow indicates tumors. Tissue:Blood of [^{89}Zr]Zr-3,2-HOPO-MSLN-mAb (HOPO, 4.5 μg , control) in HT29-MSLN xenografts 3 d after receiving coinjections of [^{89}Zr]Zr-3,2-HOPO-MSLN-mAb (180 μg , blocking); (E) each bar represents the mean Tissue:Blood ratios \pm SD ($n=5-6$ for each group).

Biodistribution of the [^{89}Zr]Zr-3,2-HOPO-MSLN-mAb in HT29-MSLN xenograft was further compared with the biodistribution of [^{89}Zr]Zr-DFO-MSLN-mAb in the same tumor model (see Supplementary Table 2 for full biodistribution data). Over 6 d [^{89}Zr]Zr-DFO-MSLN-mAb either remained fairly constant (liver) or cleared rapidly from the nontarget tissue except for the femurs (Fig. 5A). Compared with day 1 (day 1: 3.57%ID/g), femur uptake of [^{89}Zr]Zr-DFO-MSLN-mAb increased at day 3 (day 3: 4.85%ID/g) and day 6 (day 6: 6.51%ID/g). However, when compared with [^{89}Zr]Zr-3,2-HOPO-MSLN-mAb, femur uptake of [^{89}Zr]Zr-DFO-MSLN-mAb was significantly (~ 2 - to 3.5-fold, $p < 0.05$) lower over the study period (Fig. 5A). Moreover, femur T:B ratios (2.5- to 5-fold; Fig. 5B) and femur T:M ratios (2.3- to 5.5-fold; Fig. 5C) were higher for [^{89}Zr]Zr-3,2-HOPO-MSLN-mAb (T:B: 0.37–5.06; T:M: 6.98–22.21) than [^{89}Zr]Zr-DFO-MSLN-mAb (T:B: 0.15–1.14; T:M: 1.98–11.39) at all times.

Collectively, the data demonstrate decreased tumor accumulation of radiolabeled 3,2-HOPO conjugate *in vivo* in comparison with radiolabeled DFO conjugate. Tumor uptake of [^{89}Zr]Zr-DFO-MSLN-mAb (day 1: 28.04%ID/g; day 3: 33.42%ID/g; day 6: 28.49%ID/g) was found to be ~ 2.5 - to 3.5-fold higher than tumor uptake of [^{89}Zr]Zr-3,2-HOPO-MSLN-mAb. Similarly, T:B (1.11–4.59) and T:M (14.46–40.23) tumor ratios of [^{89}Zr]Zr-DFO-MSLN-mAb were

higher compared with [^{89}Zr]Zr-3,2-HOPO-MSLN-mAb. The biodistribution patterns of both the conjugates in HT29-MSLN xenografts were further confirmed by PET/CT imaging results (Fig. 5D).

Images obtained with [^{89}Zr]Zr-DFO-MSLN-mAb at days 1, 3, and 6 showed higher radioactivity in tumors compared with the images obtained with [^{89}Zr]Zr-3,2-HOPO-MSLN-mAb. Similar to the biodistribution studies, PET/CT images also displayed an increased uptake in the bone (joints and along the spinal cord; Fig. 5D) with [^{89}Zr]Zr-3,2-HOPO-MSLN-mAb vs [^{89}Zr]Zr-DFO-MSLN-mAb.

In a separate *in vivo* study, biodistribution of [^{89}Zr]Zr-3,2-HOPO-MSLN-mAb and [^{89}Zr]Zr-DFO-MSLN-mAb was performed in NCI-Meso16 and NCI-Meso21 xenografts, and compared with biodistribution of the conjugates in HT29-MSLN tumor models (Fig. 6A). Less radioactivity was measured in the blood of mice administered with [^{89}Zr]Zr-3,2-HOPO-MSLN-mAb compared with [^{89}Zr]Zr-DFO-MSLN-mAb (see Supplementary Table 3 for full biodistribution data).

For both conjugates, there was a difference in the amount of radioactivity measured in blood for different tumor types. This difference may result from the disparity in the amount of MSLN shed from each tumor in the blood. If the shed MSLN in the blood binds to the radioactive conjugate, it can interfere

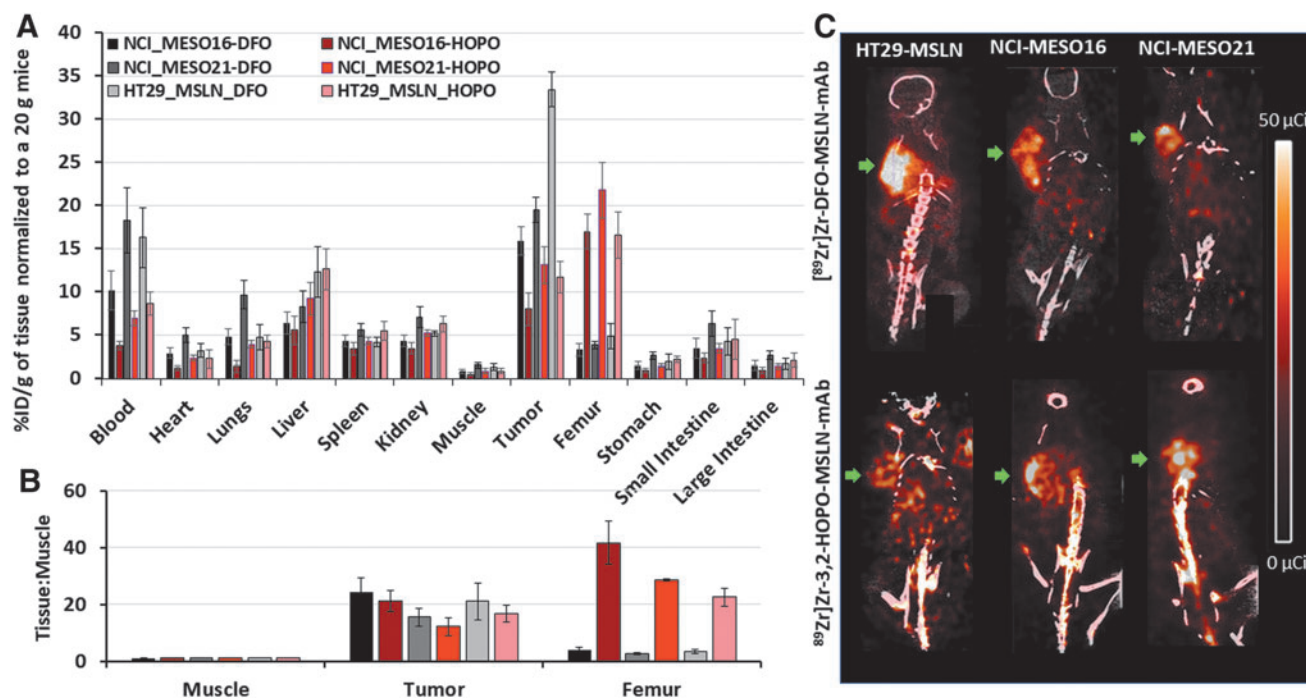


FIG. 6. Biodistribution and PET imaging. Biodistribution (A), Tissue:Muscle ratios (B), and imaging (C); representative coronal PET/CT images of [^{89}Zr]Zr-3,2-HOPO-MSLN-mAb (HOPO) and [^{89}Zr]Zr-DFO-MSLN-mAb (DFO) in HT29-MSLN, NCI-Meso16, and NCI-Meso21 mouse xenografts at day 3 postinjection of (50 μCi , 1.85 MBq; i.v) of either of the tracers. Each bar represents mean %ID/g of tissue normalized to 20 g mice \pm SE ($n=9-10$ for each point). Green arrow indicates tumors.

with the measure of the free radioactive conjugate in the blood.⁴⁰ Compared with [^{89}Zr]Zr-DFO-MSLN-mAb, [^{89}Zr]Zr-3,2-HOPO-MSLN-mAb showed 3- to 6-fold higher radioactivity in the femur in all the xenograft models (Fig. 6A).

Throughout the study, tumor T:M ratios (Fig. 6B) were slightly higher (~ 1.3 -fold) for [^{89}Zr]Zr-DFO-MSLN-mAb compared with [^{89}Zr]Zr-3,2-HOPO-MSLN-mAb in all tumor types. Contrary to tumor T:M, femur T:M ratios (Fig. 6B) of radioactive 3,2-HOPO conjugate were 6- to 10-fold higher than the radioactive DFO conjugate in all the three tumor models, suggesting the lower stability of the 3,2-HOPO chelate. Compared with [^{89}Zr]Zr-3,2-HOPO-MSLN-mAb, [^{89}Zr]Zr-DFO-MSLN-mAb consistently exhibited higher tumor uptake in all the three cancer models. Uptake (%ID/g) of [^{89}Zr]Zr-DFO-MSLN-mAb in NCI-Meso16, NCI-Meso21, and HT29-MSLN tumors was 15.88, 19.49, and 33.41, respectively. Uptake of [^{89}Zr]Zr-3,2-HOPO-MSLN-mAb in the three different tumors was found to be 7.95%ID/g (NCI-Meso16), 13.07%ID/g (NCI-Meso21), and 11.67%ID/g (HT29-MSLN).

Furthermore, imaging results in all three tumor xenografts (Fig. 6C) parallel the findings of day 3 biodistribution studies (Fig. 6A, B). The [^{89}Zr]Zr-3,2-HOPO-MSLN-mAb PET/CT images demonstrated considerably higher uptake in bones (joints and spinal cord) than that observed in [^{89}Zr]Zr-DFO-MSLN-mAb PET/CT images.

Discussion

In the present work, we synthesized and evaluated zirconium-89 labeled 3,2-HOPO-MSLN-mAb and DFO-

MSLN-mAb both *in vitro* and *in vivo*. The radiochemical yield for [^{89}Zr]Zr-3,2-HOPO-MSLN-mAb was slightly lower (80%–85%) than that for [^{89}Zr]Zr-DFO-MSLN-mAb (90%–95%) under the same conditions. However, the amount of higher molecular weighted radiochemical aggregate was higher (30%) for [^{89}Zr]Zr-3,2-HOPO-MSLN-mAb compared with [^{89}Zr]Zr-DFO-MSLN-mAb (5%–18%). To obtain comparable radiochemical aggregates as [^{89}Zr]Zr-DFO-MSLN-mAb, a lower concentration of 3,2-HOPO-MSLN-mAb per radiolabeling reaction was used. The lower radiochemical yield and purity of HOPO complexes have also been reported by Marik et al. for 3-hydroxypyridin-2-one (3,2-HOPO)-based dimacrocyclic ligand.²²

Both radiolabeled conjugates exhibited a high binding affinity for MSLN in all three cancer cell lines. Pharmacokinetics over the time course was similar for both the zirconium-89 labeled conjugates except for tumor and femur. As such, the *in vivo* biodistribution and PET/CT imaging studies demonstrated that [^{89}Zr]Zr-DFO-MSLN-mAb exhibited 2.5- to 3.5-fold higher tumor uptake compared with [^{89}Zr]Zr-3,2-HOPO-MSLN-mAb over 6 d.

Higher bone uptake with [^{89}Zr]Zr-3,2-HOPO-MSLN-mAb conjugate is suggestive of the release of free zirconium-89(IV).^{38,39} In addition, the difference in the overall charge and hydrophobicity of both the radioactive conjugates may contribute toward their diverse femur distribution.⁴¹ *In vitro*, human serum stability studies indicated that [^{89}Zr]Zr-3,2-HOPO-MSLN-mAb was less stable compared with [^{89}Zr]Zr-DFO-MSLN-mAb, with the caveat that the degradation products of the conjugates were not specifically identified.

It is important to mention that the biodistribution pattern of 3,2-HOPO-MSLN-mAb complexed to thorium-227 in HT29-MSLN tumor and femur was more similar to [⁸⁹Zr]Zr-DFO-MSLN-mAb than [⁸⁹Zr]Zr-3,2-HOPO-MSLN-mAb.¹¹ It is also necessary to acknowledge that 3,2-HOPO forms a stable complex with thorium-227, the α -radionuclide used to develop [²²⁷Th]Th-3,2-HOPO-MSLN-mAb therapeutic antibody conjugate.^{11,21}

Nonspecific accumulation of radioactivity in the bone is highly undesirable.⁴² For instance, it can lead to (I) increased radiation dose to the bone marrow if this pattern is also seen in the thorium-227 antibody conjugate, and (II) possible interference with diagnosis and interpretation of cancer lesions metastasized to bones.^{42,43} Thus, it is important that the zirconium-89(IV) forms a stable complex with the chelate *in vivo*, and the conjugate exhibits biological stability in blood serum.

3,2-HOPO-based ligands belong to a class of octadentate chelators known as hydroxypyridinones, and various hydroxypyridinones or its modified version have been evaluated for their efficiency to chelate zirconium-89(IV).^{20,42,44–47} In a study, dimacrocyclic 3,2-HOPO chelate was conjugated to trastuzumab and compared with trastuzumab-DFO conjugate.²² *In vitro* serum stability indicated the percentage of intact 3,2-HOPO-based trastuzumab conjugate dropped to ~50% within the first 24 h. *In vivo* dimacrocyclic 3,2-HOPO labeled with zirconium-89 showed more radioactivity retained in the bone than DFO-based zirconium-89 complex.

The findings of this study align with the results of our studies. In addition to HOPO- and DFO-based chelators, other compounds such as hydroxyisophthalimide- and tetraazamacrocyclic-based ligands have been evaluated as zirconium-89 chelators to develop PET agents.^{48–50}

When plausible it is preferred that the same antibody conjugate is used to analyze the biodistribution in normal organs and lesion uptake as the one used to develop the therapeutic conjugate.⁵¹ Therefore, this study intended to compare the biodistribution of [⁸⁹Zr]Zr-3,2-HOPO-MSLN-mAb and [⁸⁹Zr]Zr-DFO-MSLN-mAb. Findings of this study comparing [⁸⁹Zr]Zr-3,2-HOPO-MSLN-mAb and [⁸⁹Zr]Zr-DFO-MSLN-mAb suggest that even though [⁸⁹Zr]Zr-3,2-HOPO-MSLN-mAb can accumulate in tumors expressing high levels of MSLN, its utility in detecting low-density MSLN tumor lesions might be limited. Moreover, the higher bone uptake of [⁸⁹Zr]Zr-3,2-HOPO-MSLN-mAb may interfere with the identification of any bone metastasis.

Conclusion

[⁸⁹Zr]Zr-DFO-MSLN-mAb showed a higher tumor and lower femur uptake than [⁸⁹Zr]Zr-3,2-HOPO-MSLN-mAb. However, because [⁸⁹Zr]Zr-3,2-HOPO-MSLN-mAb uses the same chelator as [²²⁷Th]Th-3,2-HOPO-MSLN-mAb, the same zirconium-89 labeled 3,2-HOPO-MSLN-mAb conjugate could be better at studying organ distribution and lesion uptake of the MSLN-TTC, with the caveat that detection of MSLN-positive tumors in the lower extremity might be more difficult if high femur uptake is also seen in humans.

Authorship Confirmation Statement

J.R. contributed to study conception and design, conducting experiment and acquiring data, analyzing and in-

terpreting data, drafting the article, and critical revision; E.M.J. contributed to study conception and design, conducting experiment and acquiring data, review data, drafting the article, and critical revision; F.B. and O.V. contributed to synthesis and radiolabeling of antibody zirconium-89 conjugates, and critical revision; T.E.P., K.W., A.T.T., and P.L.C. contributed to conducting experiment and acquiring data, and critical revision; U.B.H. contributed to study conception and design, review data, and critical revision; A.S.C. and P.E.C. contributed to review data and critical revision; R.H. contributed to study conception and design, and critical revision; F.I.L. contributed to study conception and design, review data, drafting the article, and critical revision.

As a corresponding author of this article (F.I.L.), I confirm that all the coauthors have approved this article as submitted.

Disclosure Statement

A.S.C. holds a patent on 3,2-HOPO-MSLN-mAb conjugate. Other authors declare that he/she has no potential conflict of interest.

Funding Information

This project was funded in part by federal funds from the National Cancer Institute, National Institutes of Health (1ZIABC011825) and in part by Bayer AG, Germany. The content of this publication does not necessarily reflect the views or policies of the Department of Health and Human Services, nor does mention of trade names, commercial products, or organizations imply endorsement by the U.S. Government.

Supplementary Material

Supplementary Data
 Supplementary Table S1
 Supplementary Table S2
 Supplementary Table S3
 Supplementary Figure S1
 Supplementary Figure S2

References

- Hagemann UB, Wickstroem K, Hammer S, et al. Advances in precision oncology: Targeted Thorium-227 conjugates as a new modality in targeted alpha therapy. *Cancer Biother Radiopharm* 2020;35:497.
- Huang RX, Zhou PK. DNA damage response signaling pathways and targets for radiotherapy sensitization in cancer. *Signal Transduct Target Ther* 2020;5:60.
- Tafreshi NK, Doligalski ML, Tichacek CJ, et al. Development of targeted alpha particle therapy for solid tumors. *Molecules* 2019;24:4314.
- Kozempel J, Mokhodoeva O, Vlk M. Progress in Targeted Alpha-Particle Therapy. What we learned about recoils release from *in vivo* generators. *Molecules* 2018;23:581.
- Targeted Alpha Therapy Working G, Parker C, Lewington V, et al. Targeted alpha therapy, an emerging class of cancer agents: A review. *JAMA Oncol* 2018;4:1765.
- Elqvist J, Frost S, Pouget JP, et al. The potential and hurdles of targeted alpha therapy - clinical trials and beyond. *Front Oncol* 2014;3:324.

7. Allen BJ, Raja C, Rizvi S, et al. Targeted alpha therapy for cancer. *Phys Med Biol* 2004;49:3703.
8. Brechbiel MW. Targeted alpha-therapy: Past, present, future? *Dalton Trans* 2007;43:4918.
9. Dahle J, Borrebaek J, Jonasdottir TJ, et al. Targeted cancer therapy with a novel low-dose rate alpha-emitting radio-immunoconjugate. *Blood* 2007;110:2049.
10. Wickstroem K, Hagemann UB, Cruciani V, et al. Synergistic effect of a mesothelin targeted thorium-227 conjugate in combination with DNA damage response inhibitors in ovarian cancer xenograft models. *J Nucl Med* 2019;60:1293.
11. Hagemann UB, Ellingsen C, Schuhmacher J, et al. Mesothelin-Targeted Thorium-227 Conjugate (MSLN-TTC): Preclinical evaluation of a new targeted alpha therapy for mesothelin-positive cancers. *Clin Cancer Res* 2019; 25:4723.
12. Hagemann UB, Mihaylova D, Uran SR, et al. Targeted alpha therapy using a novel CD70 targeted thorium-227 conjugate in vitro and in vivo models of renal cell carcinoma. *Oncotarget* 2017;8:56311.
13. Heyerdahl H, Abbas N, Brevik EM, et al. Fractionated therapy of HER2-expressing breast and ovarian cancer xenografts in mice with targeted alpha emitting 227Th-DOTA-p-benzyl-trastuzumab. *PLoS One* 2012;7:e42345.
14. Dahle J, Larsen RH. Targeted alpha-particle therapy with Th-227-labeled antibodies. *Curr Radiopharm* 2008;1:209.
15. Hagemann UB, Wickstroem K, Wang E, et al. In vitro and in vivo efficacy of a novel CD33-Targeted Thorium-227 conjugate for the treatment of acute myeloid leukemia. *Mol Cancer Ther* 2016;15:2422.
16. Baldo P, Cecco S. Amatuximab and novel agents targeting mesothelin for solid tumors. *Onco Targets Ther* 2017;10: 5337.
17. Hassan R, Thomas A, Alewine C, et al. Mesothelin immunotherapy for cancer: Ready for prime time? *J Clin Oncol* 2016;34:4171.
18. Tchou J, Wang LC, Selven B, et al. Mesothelin, a novel immunotherapy target for triple negative breast cancer. *Breast Cancer Res Treat* 2012;133:799.
19. Illei PB, Alewine C, Zahurak M, et al. Mesothelin expression in advanced gastroesophageal cancer represents a novel target for immunotherapy. *Appl Immunohistochem Mol Morphol* 2016;24:246.
20. Ramdahl T, Bonge-Hansen HT, Ryan OB, et al. An efficient chelator for complexation of thorium-227. *Bioorg Med Chem Lett* 2016;26:4318.
21. Deblonde GJP, Lohrey TD, Booth CH, et al. Solution Thermodynamics and kinetics of metal complexation with a hydroxypyridinone chelator designed for Thorium-227 targeted alpha therapy. *Inorg Chem* 2018;57:14337.
22. J NT, Pandya DN, Pailloux SL, et al. Evaluation of a 3-hydroxypyridin-2-one (2,3-HOPO) Based Macrocyclic Chelator for (89)Zr(4+) and Its Use for ImmunoPET imaging of HER2 positive model of ovarian carcinoma in mice. *Theranostics* 2016;6:511.
23. Buchwalder C, Rodriguez-Rodriguez C, Schaffer P, et al. A new tetrapodal 3-hydroxy-4-pyridinone ligand for complexation of (89)zirconium for positron emission tomography (PET) imaging. *Dalton Trans* 2017;46:9654.
24. O'Donoghue JA, Lewis JS, Pandit-Taskar N, et al. Pharmacokinetics, biodistribution, and radiation dosimetry for (89)Zr-Trastuzumab in patients with esophagogastric cancer. *J Nucl Med* 2018;59:161.
25. Sharma SK, Sevak KK, Monette S, et al. Preclinical Zr-89 Immuno-PET of High-grade serous ovarian cancer and lymph node metastasis. *J Nucl Med* 2016;57:771.
26. Vosjan MJWD, Perk LR, Visser GWM, et al. Conjugation and radiolabeling of monoclonal antibodies with zirconium-89 for PET imaging using the bifunctional chelate p-isothiocyanatobenzyl-desferrioxamine. *Nat Protocols* 2010;5:739.
27. Berg E, Gill H, Marik J, et al. Total-Body PET and Highly Stable Chelators Together Enable Meaningful Zr-89-Antibody PET Studies up to 30 Days After Injection. *J Nucl Med* 2020;61:453.
28. Brandt M, Cowell J, Aulsebrook ML, et al. Radiolabelling of the octadentate chelators DFO* and oxoDFO* with zirconium-89 and gallium-68. *J Biol Inorg Chem* 2020;25: 789.
29. Raave R, Sandker G, Adumeau P, et al. Direct comparison of the in vitro and in vivo stability of DFO, DFO* and DFOcyclo* for Zr-89-immunoPET. *Eur J Nucl Med Mol Imaging* 2019;46:1966.
30. Boros E, Packard AB. Radioactive transition metals for imaging and therapy. *Chem Rev* 2019;119:870.
31. Brandt M, Cardinale J, Aulsebrook ML, et al. An Overview of PET Radiochemistry, Part 2: Radiometals. *J Nucl Med* 2018;59:1500.
32. Vugts DJ, Klaver C, Sewing C, et al. Comparison of the octadentate bifunctional chelator DFO*-pPhe-NCS and the clinically used hexadentate bifunctional chelator DFO-pPhe-NCS for Zr-89-immuno-PET. *Eur J Nucl Med Mol Imaging* 2017;44:286.
33. Jagoda EM, Vasalatiy O, Basuli F, et al. Immuno-PET Imaging of the Programmed Cell Death-1 Ligand (PD-L1) Using a Zirconium-89 labeled therapeutic antibody, avelumab. *Mol Imaging* 2019;18:1536012119829986.
34. Meares CF, Mccall MJ, Reardan DT, et al. Conjugation of antibodies with bifunctional chelating-agents - isothiocyanate and bromoacetamide reagents, methods of analysis, and subsequent addition of metal-ions. *Anal Biochem* 1984;142:68.
35. Morris BJ. Specific radioactivity of radioimmunoassay tracer determined by self-displacement: A re-evaluation. *Clin Chim Acta* 1976;73:213.
36. Kalra N, Zhang JL, Thomas A, et al. Mesothelioma patient derived tumor xenografts with defined BAP1 mutations that mimic the molecular characteristics of human malignant mesothelioma. *BMC Cancer* 2015;15:376.
37. Reddy N, Ong GL, Behr TM, et al. Rapid blood clearance of mouse IgG2a and human IgG1 in many nude and nu/+ mouse strains is due to low IgG2a serum concentrations. *Cancer Immunol Immunother* 1998;46:25.
38. Abou DS, Ku T, Smith-Jones PM. In vivo biodistribution and accumulation of 89Zr in mice. *Nucl Med Biol* 2011;38: 675.
39. Fischer G, Seibold U, Schirmmacher R, et al. (89)Zr, a radiometal nuclide with high potential for molecular imaging with PET: Chemistry, applications and remaining challenges. *Molecules* 2013;18:6469.
40. Lee JH, Kim H, Yao Z, et al. Tumor-shed antigen affects antibody tumor targeting: Comparison of Two (89)Zr-labeled antibodies directed against shed or nonshed antigens. *Contrast Media Mol Imaging* 2018;2018:2461257.
41. Tabrizi M, Bornstein GG, Suria H. Biodistribution mechanisms of therapeutic monoclonal antibodies in health and disease. *AAPS J* 2010;12:33.

42. Heskamp S, Raave R, Boerman O, et al. (89)Zr-Immuno-Positron Emission Tomography in Oncology: State-of-the-Art (89)Zr Radiochemistry. *Bioconjug Chem* 2017;28:2211.
43. Deri MA, Zeglis BM, Francesconi LC, et al. PET imaging with (8)(9)Zr: From radiochemistry to the clinic. *Nucl Med Biol* 2013;40:3.
44. Deri MA, Ponnala S, Zeglis BM, et al. Alternative Chelator for Zr-89 Radiopharmaceuticals: Radiolabeling and Evaluation of 3,4,3-(LI-1,2-HOPO). *J Med Chem* 2014;57:4849.
45. Deri MA, Ponnala S, Kozowski P, et al. p-SCN-Bn-HOPO: A Superior Bifunctional Chelator for Zr-89 ImmunoPET. *Bioconjug Chem* 2015;26:2579.
46. Bhatt NB, Pandya DN, Wadas TJ. Recent Advances in Zirconium-89 chelator development. *Molecules* 2018;23:638.
47. Guerard F, Beyler M, Lee YS, et al. Investigation of the complexation of Zr-nat(IV) and Zr-89(IV) by hydroxypyridinones for the development of chelators for PET imaging applications. *Dalton Trans* 2017;46:4749.
48. Pandya D, Bhatt N, Day C, et al. Zirconium-89 tetraazamacrocyclic complexes: The influence of macrocyclic structure on stability. *J Nucl Med* 2018;59:252.
49. Pandya DN, Bhatt N, Yuan H, et al. Zirconium tetraazamacrocyclic complexes display extraordinary stability and provide a new strategy for zirconium-89-based radiopharmaceutical development. *Chem Sci* 2017;8:2309.
50. Bhatt NB, Pandya DN, Xu JD, et al. Evaluation of macrocyclic hydroxyisophthalamide ligands as chelators for zirconium-89. *PLoS One* 2017;12:e0178767.
51. Moek KL, Giesen D, Kok IC, et al. Theranostics using antibodies and antibody-related therapeutics. *J Nucl Med* 2017;58:83S.